Soft Matter

PAPER

View Article Online
View Journal | View Issue



Cite this: *Soft Matter*, 2020, **16**, 3224

# Distinct dynamics of structural relaxation in the amorphous phase of poly(L-lactic acid) revealed by quiescent crystallization†

Xavier Monnier, ‡ Nicolas Delpouve * and Allisson Saiter-Fourcin

Received 29th December 2019,
Accepted 23rd February 2020

DOI: 10.1039/c9sm02541c

rsc.li/soft-matter-journal

Fast scanning calorimetry (FSC) experiments were performed to investigate physical aging in amorphous and semi-crystalline poly(L-lactic acid)s (PLLAs) that were thermally crystallized under conditions leading to the α′- or α-crystalline form, and either favouring or inhibiting the development of a rigid amorphous fraction (RAF). The enthalpy of recovery was calculated after two procedures of rescaling to the content of the whole amorphous phase and also to the only content of the mobile amorphous fraction (MAF), which helped in clarifying the contribution of the RAF. From the dependence of the structural relaxation rate on the aging temperature, two regimes were evidenced for all samples. In the aging temperature domain situated close to the glass transition, the structural relaxation occurs significantly faster in the MAF. Its rate is independent of the aging temperature and is not influenced by the microstructure. However, the distance to equilibrium is higher in samples for which the coupling is strong between crystal and amorphous, implying that the time to reach equilibrium is also higher. In contrast, at low aging temperatures, for which the whole amorphous phase can be considered as solid, MAF and RAF exhibit the same structural relaxation rate. This convergence in the relaxation kinetics by decreasing the temperature of physical aging was interpreted as the evolution of relaxation dynamics in the MAF from segmental to local. This change is highlighted by the comparison between MAF and RAF relaxation kinetics, but it occurs similarly in a pure amorphous system.



## 1. Introduction

Fast scanning calorimetry (FSC) has recently emerged as a powerful technique for polymer characterization. Among the results obtained thanks to FSC, some refer to topics such as crystallization kinetics,[1] crystalline reorganization,[2,3] and nucleation.[4,5] Glassy dynamics related to the structural relaxation of polymers has also been vastly explored.[6–24] Structural relaxation, or physical aging, is characterized by a change in thermodynamic quantities such as enthalpy and specific volume. During the structural relaxation, the thermodynamically out-of-equilibrium glass minimizes its thermodynamic quantities to approach equilibrium.[25–29] The distance separating a glass from equilibrium can be evaluated from the concept of fictive temperature introduced by Tool.[30] Using FSC, Gao *et al.*[7] measured the limiting fictive temperature, meaning the fictive temperature in the case of a non-aged glass,[7] over five decades of cooling and heating rates. They showed that the limiting fictive temperature is dependent on the cooling rate and is not a function of heating rate.[7] Another change in the glass structure, the departure from equilibrium, introduced by Kovacs,[31] has been studied in polystyrene by Lopez *et al.*[8] They performed intrinsic isotherm, asymmetry of approach, and memory effect experiments[8] (experiments historically performed by Kovacs[31] that demonstrated the nonlinear and nonexponential character of structural relaxation). They obtained, thanks to FSC, the complete response of these three signatures of structural recovery in enthalpy space.[8] Recently, Grassia *et al.*[24] have fitted the experimental data obtained by FSC for polystyrene with a new modified version of the Tool–Narayanaswamy–Moynihan model.[32–34]

Depending on their distance to equilibrium, the stability of glasses differs. For example, highly stable glasses can be obtained by physical vapour deposition of organic molecules.[35,36] Yoon *et al.*[18] have prepared by vacuum pyrolysis deposition 300 to 700 nm thick ultrastable amorphous fluoropolymer glasses.

*Normandie Univ, UNIROUEN Normandie, INSA Rouen, CNRS, Groupe de Physique des Matériaux, 76000 Rouen, France. E-mail: nicolas.delpouve1@univ-rouen.fr; Fax: +33 (0)232955082; Tel: +33 (0)232955165*

† Electronic supplementary information (ESI) available: Details regarding the calculation of the degree of crystallinity, the glass transition temperature determined upon cooling, the onset of structural relaxation, the FSC curves obtained by aging for 10 minutes amorphous and semi-crystalline PLLAs, and the enthalpy of recovery dependence on temperature prior to rescaling. See DOI: 10.1039/c9sm02541c

‡ Present address: Centro de Física de Materiales (CSIC-UPV/EHU) & Donostia International Physics Center (DIPC), Paseo Manuel de Lardizábal 4, 20018 SanSebastián, Spain.

They report a 57 °C reduction of the fictive temperature in these ultrastable glasses compared to the nominal glass transition. Mc Kenna *et al.* investigated structural relaxation in ultrastable amorphous Teflon.[19] They reported deviations from VFT toward a higher activation energy Arrhenius-like behaviour, similar to previous results obtained on amber.[37] Monnier *et al.*[38] obtained thermodynamic states, with a fictive temperature 80 °C below the polymer glass transition temperature, in glassy poly(4-*tert*-butylstyrene) confined at the micrometer length scale. They correlated the access to these thermodynamic states to a fast equilibration mechanism, promoted by the large amount of free interface.[39,40] Fast equilibration mechanisms based on enhancing the amount of free interface were also exploited by Boucher *et al.*,[41] who reported the fictive temperature to reach the predicted Kauzmann temperature value in 30 nm stacked PS films.

The possibility for a polymer glass to reach the extrapolated liquid line has been contested in some past studies.[42–45] It has, for example, been assumed that the structural relaxation was hindered because of chain entanglement and steric hindrance.[46] Nevertheless, Koh *et al.*[47] have presented measurements of the enthalpy recovery of polystyrene, 15 °C below the nominal glass transition temperature, for aging times up to 1 year, and showed that the equilibrium enthalpy line can be reached. In addition, among recent studies, some show that physical aging occurs *via* a single step process toward equilibrium,[8,9,47] whereas others report the existence of a plateau,[48,49] and two different mechanisms of equilibration.[50–53] Data obtained from FSC regarding this question are provided in previous studies.[8,9,51] In this context, one of the main advantages of FSC, when it comes to physical aging study, is that the very high cooling rates that are possibly used, about 1000 K $s^{-1}$, increase the temperature for which the liquid-like state is quitted in comparison to what is possible using classical differential scanning calorimetry (DSC).[10,12] Thus, aging investigations from FSC can be performed at temperatures that are hardly accessible from DSC, and for which the time to reach equilibrium is shorter due to the high mobility of the chains. FSC experiments show, for aging times compatible with *in situ* experiments, the possibility for a polymer glass to reach the extrapolated liquid line.[8,11,54] Moreover, at a given aging temperature, so for a given equilibration time, the glass formed at a high cooling rate by FSC is at a higher distance to the liquid-like equilibrium line. Therefore, it is possible to conjugate two conditions that facilitate the observation of any effect impacting the kinetics of physical aging: a short equilibration time and high distance to equilibrium.

In this work, we use FSC to investigate the impact of crystallization conditions on the structural relaxation mechanism of poly(L-lactic acid) (PLLA). PLLA is likely one of the more reliable semi-crystalline biopolymers to replace petroleum-based polymers for longer life-time applications despite its brittleness and low thermal resistance.[55] Its dimensional stability during service should also be considered.[56] In particular, and because poly(lactic acid)s (PLAs) exhibit a glass transition temperature, about 60 °C, which is slightly above their temperature of use, generally ambient or human body temperature,[57] PLLA is strongly sensitive to the structural relaxation. Several results were recently obtained from PLLA physical aging. Androsch and Di Lorenzo[58] evidenced a nucleation mechanism below the glass transition temperature. Di Lisio *et al.*[59] showed from modulated temperature FTIR spectroscopy that the structural relaxation is dependent on the conformer distribution in the liquid before its vitrification. Cui *et al.*[60] investigated the mechanical properties of injection moulded aged PLA. Monnier *et al.* investigated the structural relaxation kinetics of PLAs in amorphous samples,[11,16] under quiescent and flow-induced crystallization conditions,[61] and in polystyrene/polylactide multilayer films.[17]

As for many polymers,[62–65] the decoupling between both amorphous and crystalline phases is imperfect in PLLA, so a rigid amorphous fraction (RAF) forms.[66] In this part of the amorphous phase, the molecular mobility is highly restrained, leading its devitrification to occur significantly above the glass transition.[67] In a recent study,[68] the participation of RAF in the physical aging process at high undercooling has been assumed.

Furthermore, in PLLA, the coupling differs depending on the crystallization conditions, and is associated with polymorphism. By annealing above 120 °C, the most stable polymorph, the α-form, is created.[69] Crystallization below 100 °C leads to a more disordered form, the α′-form,[69–71] which is characterized by a looser chain packing and slightly larger unit cell dimensions.[72] These latter annealing conditions induce a local increase in free volume,[73] related to strong coupling. The idea of this work is to confront, for different quiescent crystallization conditions, the theoretically antagonistic effects on the aging kinetics caused, respectively, by the crystalline phase nature and the local dedensification of the amorphous phase associated with the RAF.

## 2. Experimental

### 2.1 Materials

PLLA pellets were purchased from PURAC®, Corbion, Netherlands (PURASORB PL24® GMP commercial grade of homopolymer). Average molecular weight in number $M_n$ = 59 500 g $mol^{-1}$ and the polydispersity index $I_p$ = 1.8 were provided in a previous study.[74] Before any experiment, PLLA pellets were heated at 50 °C to remove residual humidity.

### 2.2 Polarized optical microscopy (POM)

Polarized optical microscopy (POM) images were obtained in transmission and reflection modes, for bulk PLLA and PLLA on the FSC chip respectively, using a universal EPI-illuminator® polarized optical microscope equipped with Nikon M Plan ×5 objective lenses, and connected with a digital camera system from Nikon Corporation®. To observe the appearance and growth of spherulites during isothermal crystallization, the samples were heated on a hot stage Mettler FP 82®.

### 2.3 Fast scanning calorimetry (FSC)

Fast scanning calorimetry (FSC) investigations were carried out on Flash DSC 1 (Mettler Toledo®) apparatus equipped with a

Huber TC100® intra-cooler. PLLA pellets were cut into slices using a microtome. The samples were positioned on the sensitive area of a MultiSTAR UFS 1 MEMS® chip sensor. Prior to use, the chip was conditioned and corrected according to Mettler Toledo® procedures. Following the recommendation of Toda *et al.*,[75] samples with thickness less than 10 μm were prepared to prevent a thermal gradient. The adhesion of the PLLA sample onto the chip was promoted by adding a thin layer of silicon oil, thus improving thermal contact. Prior to any experiment, a good thermal contact was ensured by consecutive heating and cooling at 1000 K $s^{-1}$, up to 250 °C, and down to −80 °C. The sample was positioned in the middle area of the sensor, where the temperature distribution is the most homogeneous, as shown by Jariyavidyanont *et al.*[76]

Experiments were performed under a 20 mL $min^{-1}$ nitrogen flow. Sample mass was estimated from the step change in heat flow at the glass transition by assuming that the heat capacity step value ΔCp of PLLA obtained by FSC at $|\beta_c| = \beta_h = 1500$ K $s^{-1}$ is identical to the value obtained by modulated temperature differential scanning calorimetry (MT-DSC) at $\beta_h = 2$ K $min^{-1}$. The mass of the samples ranged between 60 and 80 ng. The calibration procedure of FSC has been previously detailed,[17] and it includes the correction of both static and dynamic thermal lags following the equations recommended by Schawe.[77] Experiments were repeated twice.

### 2.4 Crystallization procedures

Amorphous PLLA samples were obtained by cooling from the melt temperature down to ambient temperature at 1500 K $s^{-1}$. Crystallization from melt was performed by cooling the sample at 1500 K $s^{-1}$ down to $T_c$. Crystallization from glass was performed by successively cooling the sample down to −60 °C at 1500 K $s^{-1}$ then heating it up to $T_c$ at the same rate. Crystallization time $t_c$ ranged between 1 and 600 min. After crystallization, the sample was cooled down to −60 °C at 1500 K $s^{-1}$. The subsequent FSC scan was also performed at 1500 K $s^{-1}$. Crystallization temperatures, 89 and 149 °C, were chosen to maximize the selective formation of the α′- and α-polymorph, respectively.

The degree of crystallinity $X_c$ of PLLA was calculated by:

$$X_c = \frac{\Delta H_m - \sum \Delta H_c}{\Delta H_m^\circ} \quad (1)$$

where $\Delta H_m$ is the enthalpy of melting, $\Delta H_c$ is the enthalpy of cold crystallization, and $\Delta H_m^\circ$ is the theoretical enthalpy of melting of the totally crystalline polymer. $\Delta H_c$ is equal to zero when the heating rate is fast enough to prevent any cold crystallization or reorganization, which is the case in this study. In the present study, we used the temperature dependence of $\Delta H_m^\circ$ proposed by Righetti *et al.*,[78] which leads to $\Delta H_m^\circ = 111.1$ J $g^{-1}$ for α′-crystals melting at $T_m = 160$ °C and $\Delta H_m^\circ = 149.7$ J $g^{-1}$ for α-crystals melting at $T_m = 200$ °C. The RAF content, noted as $X_{RAF}$, was then calculated from:

$$X_{RAF} = 1 - (X_C + X_{MAF}) \text{ with } X_{MAF} = \frac{\Delta Cp}{\Delta Cp^\circ} \quad (2)$$

where $X_{MAF}$ is the content of mobile amorphous fraction and $\Delta Cp^\circ$ is the heat capacity step associated with the glass transition of fully amorphous PLLA.

### 2.5 Physical aging

Physical aging kinetics was investigated on amorphous and semi-crystalline PLLAs by means of FSC. Two sets of physical aging experiments have been performed. In the first set, the structural relaxation process has been investigated for a given aging time $t_{ag} = 10$ minutes at different temperature $T_{ag}$ ranging from 72 down to −3 °C. In the second set, two aging temperatures, respectively 50 and 63 °C, have been chosen. Then, the physical aging experiments were performed with the aging time $t_{ag}$ varying from 0.001 to 1000 minutes. Amorphous and semi-crystalline PLLAs (annealing procedure described in paragraph 2.4, with $t_c = 200$ min) were cooled down to −60 °C and then heated up to $T_{ag}$ at 1500 K $s^{-1}$. Consecutive to the aging step, PLLA samples underwent two consecutive cooling/heating steps at 1500 K $s^{-1}$. The first one allows getting the calorimetric signature of the aged PLLA, *i.e.*, the structural recovery,[28] while the second allows obtaining the FSC curve for a non-aged PLLA.

For amorphous and semi-crystalline PLLAs, the enthalpy of recovery $\Delta H$ ($T_{ag}$, $t_{ag}$) was calculated as reported in previous studies,[11,17,68] according to the following equation:

$$\Delta H(T_{ag}, t_{ag}) = \int_{T_1}^{T_2} \left[Cp_{aged}(T) - Cp_{non\text{-}aged}(T)\right] dT. \quad (3)$$

in which $Cp_{aged}(T)$ and $Cp_{non\text{-}aged}(T)$ are the heat flows of the aged and non-aged samples, respectively, which are normalized to both sample mass and heating rate in order to be expressed in units equivalent to specific heat capacity. $T_1$ and $T_2$ are temperatures arbitrarily chosen, and they correspond to the start and end of the thermal signature of the glass transition, with the enthalpy recovery peak superimposed, respectively. At $T_1$ and $T_2$, the values of $Cp_{aged}(T)$ and $Cp_{non\text{-}aged}(T)$ are the same. When an exotherm appears in the normalized heat flow curve prior to the appearance of the broad endothermic peak, the area of the dip has to be included in the calculation of the enthalpy of recovery.[68,79]

## 3. Results and discussion

### 3.1 Morphology and signature of the coupling between crystal and amorphous

Fig. 1 displays the pictures obtained from POM after crystallizing bulk PLLA from the melt at 89 °C (Fig. 1A) for 140 minutes and at 149 °C for 170 minutes (Fig. 1B) in the hot stage. In consistence with several authors[80–83] reporting that the size of the spherulites increases with the crystallization temperature, crystallization at 89 °C under predominant germination conditions[81] generates mostly small size spherulites with diameter less than 50 μm, whereas crystallization at 149 °C in predominant growth conditions[81] generates well-defined big spherulites with diameter about 200 μm.

 

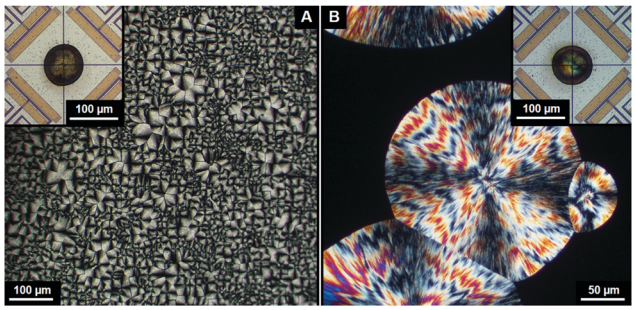


Fig. 1 Polarized optical micrographs of PLLA bulk samples crystallized from melt at $T_c$ = 89 °C for 140 minutes (A) and at $T_c$ = 149 °C for 170 minutes (B), as well as respective polarized optical micrographs of PLLA samples on the FSC chip sensor after *in situ* crystallization (insets).

In the insets of Fig. 1, the POM pictures of PLLA samples on the FSC chip sensor after *in situ* crystallization are shown. The sample diameter is close to 85 µm, slightly higher than the spherulite average diameter after crystallizing at 89 °C and less than the spherulite average diameter after crystallizing at 149 °C. Therefore, one can reasonably question the possibility to get identical microstructures in FSC compared to bulk samples. Although it is not possible to distinguish any spherulite, interestingly, the difference in crystallization conditions is reflected in the sample feature. Multiple grain-like structures similar to germs are observed after crystallization at 89 °C on the FSC chip sensor. On the other hand, one can observe a continuous coloration for the sample crystallized at 149 °C, which leads us to suppose that the sample volume is wholly invaded by one or a few spherulites. Despite the space limit in the growth of the spherulitic structure, one can assume that the morphology of FSC samples, and bulk samples, is dependent on crystallization conditions.

Fig. 2 shows the heat flow curves from FSC analyses, subsequent to the crystallization from the glass at 89 °C (Fig. 2A) and at 149 °C (Fig. 2B), for annealing times ranging from 5 up to 600 minutes and 7 up to 600 minutes, respectively. For a clear comparison between curves, the FSC heat flow curves were normalized to both scanning rate and sample mass. The focus on the glass transition, which is detected between 60 and 100 °C classically, reveals a decrease in the heat flow step with the annealing time, as the content of amorphous phase progressively decreases with the crystalline phase growth. The melting occurs at higher temperatures (onset at about 180 °C and peak maximum at about 200 °C) when crystallizing at 149 °C in comparison to crystallization at 89 °C (onset at about 140 °C and peak maximum at about 160 °C), and the enthalpy of melting is also higher. This is the expected signature of the formation of the more perfect α-form, characterized by a higher degree of perfection, when crystallizing at higher temperatures. Moreover, it is consistent with the POM pictures and with the literature,[69] reporting that the α′-form generated at 89 °C is a disordered imperfect crystalline form in comparison to the α-form generated at 149 °C.

FSC allows determining the cooling rate needed to annihilate crystalline reorganization.[84] The investigations led by

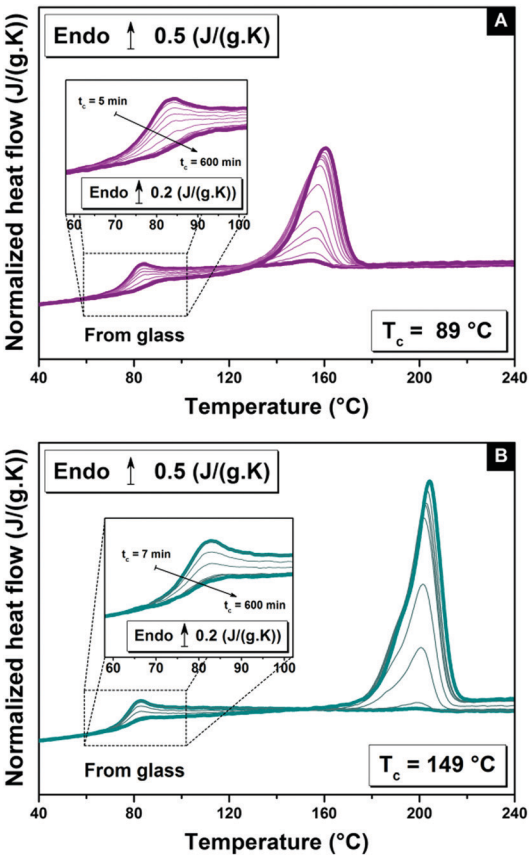


Fig. 2 Heat flow curves from fast scanning calorimetry normalized to both sample mass and heating rate of initially amorphous PLLA samples crystallized from the glass for $t_c$ = [5, 7, 10, 12, 15, 20, 30, 50, 70, 100, 200, and 600] minutes at $T_c$ = 89 °C (A) and for $t_c$ = [7, 10, 20, 30, 50, 70, 100, 200, and 600] minutes at $T_c$ = 149 °C (B). A focus on the glass transition is given in the insets.

Androsch *et al.*[85–87] show that non-isothermal nucleation can be suppressed by cooling PLLA at 50 K $s^{-1}$ and that the reorganization of the α′-form into the α-form, which is observed when performing DSC analysis at conventional heating rates, *i.e.*, about 10 K $min^{-1}$, can be prevented for heating rates higher than 30 K $s^{-1}$. Therefore, the melting peak in Fig. 2A really corresponds to the melting of α′-crystals, which is usually not observable.

The MAF and RAF contents with crystallization advancement are respectively given in Fig. 3A and B. One can observe that $X_{RAF}$ is higher by crystallizing at 89 °C, in comparison to the crystallization at 149 °C ($X_{RAF}$ = 15 ± 4% for $T_c$ = 89 °C, and 5 ± 4% for $T_c$ = 149 °C) but it does not reach a content as high as that obtained from bulk crystallization.[68] Crystallization under confinement might be detrimental for the formation of RAF as a minimum space is needed for its creation.[88] Fernandes Nassar *et al.*[89] have shown that it is possible to crystallize PLLA up to 43% without forming RAF when PLLA is confined against polystyrene in 20 nm layers obtained by a layer multiplying co-extrusion technique.

To evaluate the impact of the annealing conditions on the amorphous phase properties, the glass transition measured

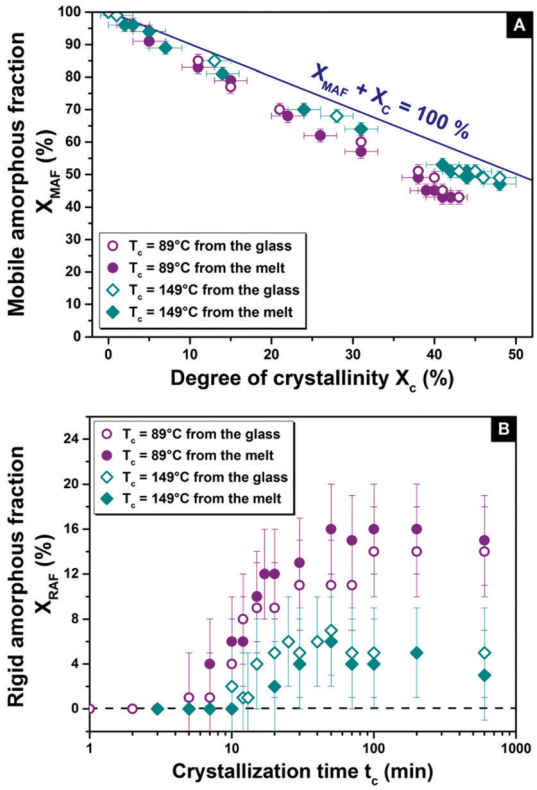


Fig. 3 Quantities of amorphous fractions during PLLA crystallization from glass and melt at 89 and 149 °C. (A) Mobile amorphous fraction *versus* degree of crystallinity. The blue line indicates the expected variations according to the two-phase model and allows quantifying the deviation from this model. (B) Rigid amorphous fraction *versus* the crystallization time. See the ESI† for more details concerning the variation of $X_c$ with $t_c$, and the influence of the chosen value for $\Delta H_m^\circ$ on the calculation of $X_{RAF}$.

upon cooling $T_{g,mid}$ has been determined for amorphous PLLA and PLLA crystallized for $t_c$ = 200 minutes, *i.e.*, for $X_c = X_{c,max}$ (see ESI†). Moreover, as shown in Fig. 4, the midpoint of the glass transition signature obtained upon heating $T_{mid\,heat}$ has also been measured for various $t_c$. The difference $T_{mid\,heat} - T_{0\,mid\,heat}$ is given as a function of $X_c$, where $T_{0\,mid\,heat}$ = 72 °C is the midpoint of the glass transition signature obtained upon heating for an amorphous PLLA. As revealed from previous studies,[72,73,90,91] low crystallization temperatures cause broadening of the MAF devitrification and the shift of its midpoint to higher temperatures. According to Fig. 4, the shift $T_{mid\,heat} - T_{0\,mid\,heat}$ with the annealing time is indeed significantly stronger, close to 12 °C after 600 minutes of annealing, when crystallizing at 89 °C, in comparison to crystallization at 149 °C, wherein it is close to 3 °C after 600 minutes of annealing.

There is no clear consensus regarding the causes for the MAF constraint, which results in the shift of the glass transition signature towards higher temperature. The microstructure of PLLA, after crystallization at low and high temperatures, has been depicted according to the heterogeneous stack model by Righetti *et al.*[72] In this model, the RAF locates in the interlamellar regions and the MAF in the larger interstack gaps.[72] Thus, the glass transition shift relates to the dimension of the

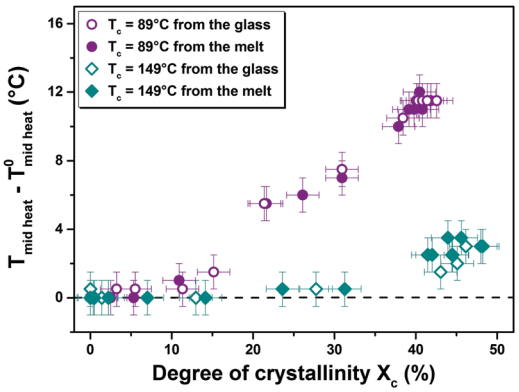


Fig. 4 Difference between $T_{mid\,heat}$ the midpoint of the glass transition signature obtained upon heating and $T_{0,mid\,heat}$ the midpoint of the glass transition signature obtained upon heating for an amorphous PLLA as a function of $X_c$ for crystallization at 89 °C and 149 °C, from both the glass and the melt.

interstack region. Androsch *et al.*[92] associated the coupling between amorphous and ordered phases with the presence of nanometer-sized ordered domains to explain the shift of the glass transition of PA11. The studies performed by Schawe[93,94] on isotactic polypropylene revealed that the RAF induces a strong increase of the glass transition, although this shift was essentially interpreted as the consequence of mobility restrictions imposed by the crystalline fraction. Esposito *et al.*[95] interpreted the shift of the glass transition towards higher temperatures as the result of gradual mobility constraints, transferring from the crystalline phase to the MAF through the RAF behaving as a buffer. Fernandes Nassar *et al.*[89] crystallized PLLA beyond 40% in PS/PLLA multi-nanolayered films. They reported, for similar confinement conditions, that the glass transition increases when $X_{RAF}$ = 25%, whereas it shifts towards lower temperatures in the absence of RAF. They concluded that the glass transition of the MAF depends on the coupling between phases. Regardless of the interpretation, Fig. 4 shows that the MAF is more constrained by crystallizing at 89 °C.

### 3.2 Structural relaxation in the mobile amorphous fraction (MAF)

It is possible using the FSC scans following the physical aging procedures to investigate the impact of the microstructure on the structural relaxation. However, the direct comparison of the enthalpy of recovery is misleading, since the quantity of PLLA relaxing at the glass transition is lower in semi-crystalline samples. Consequently, one cannot discriminate only from the determination of values of $\Delta H(T_{ag}, t_{ag})$ in semi-crystalline polymers what results from changes in relaxation dynamics such as mobility restrictions induced by crystals and what is linked to the lower content of amorphous phase. As an answer, it might be proposed to rescale the enthalpy of recovery to $X_{MAF}$, *i.e.*, the content of amorphous phase relaxing at the glass transition (see Fig. 5). The onset of structural relaxation $T^{Onset}_{Struct.,Relax.}$ was determined as detailed in the ESI.†[96] It is remarkable that the signature of

 

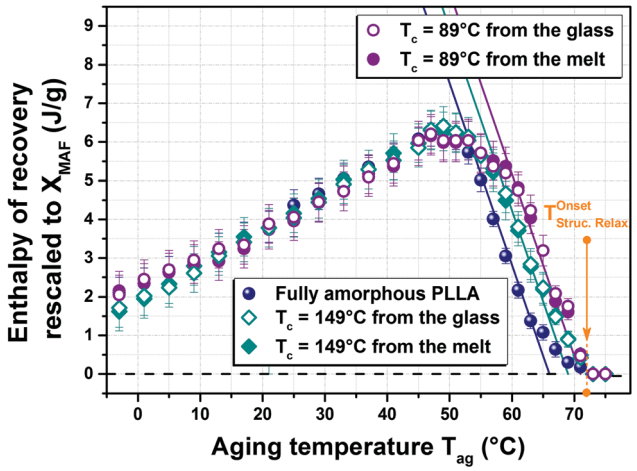


Fig. 5 Enthalpy of recovery rescaled to the content of mobile amorphous fraction as a function of aging temperature for amorphous and semi-crystalline PLLAs ($t_c$ = 200 minutes) aged for $t_{ag}$ = 10 minutes. The onset of structural relaxation at 72 °C is indicated by an arrow. The solid lines correspond to the variations of the total enthalpy loss with the aging temperature.

physical aging is detected in amorphous PLLA and, to a lesser extent, in semi-crystalline PLLA, for aging above $T_{g\,mid}$. Therefore, the structural relaxation can start in a sample not completely vitrified. The experimental values of $\Delta H$ ($T_{ag}$, $t_{ag}$ = 10 min) and the FSC curves from which these quantities were extracted are given in the ESI† (Fig. S5–S7).

The dependence of the enthalpy of recovery on the aging temperature can be fitted for all PLLA following the equation $\Delta H_\infty = \Delta Cp \times (T_{g\,mid} - T_{ag})$, where $\Delta Cp = 0.47$ J g$^{-1}$ K$^{-1}$ is the heat capacity step associated with the glass transition of amorphous PLLA calculated from MT-DSC measurements, $\Delta H_\infty$ is the total enthalpy loss, defined as the change needed in the enthalpy of recovery to reach the thermodynamic equilibrium, and $T_{g\,mid}$ is the value of the glass transition midpoint obtained upon cooling, which also corresponds to the glass transition midpoint obtained upon heating after correcting the thermal lag. For most of the aging temperatures above 50 °C, the structural relaxation occurs fast enough for reaching equilibrium in 10 minutes aging. Therefore, the equation $\Delta H_\infty = \Delta Cp \times (T_{g\,mid} - T_{ag})$ correctly fits the calculated enthalpy of recovery (Fig. 5). However, $\Delta H$ ($T_{ag}$, $t_{ag}$ = 10 min) is not linearly correlated with the aging temperature $T_{ag}$ and shows a maximum at $T_{ag}$ = 50 °C. This behaviour is generally interpreted as the consequence of antagonist effects, thermodynamic and kinetic, on the structural relaxation. On one hand, the glass is farther from thermodynamic equilibrium when decreasing $T_{ag}$, so the driving force of the structural relaxation increases with reducing the aging temperature. On the other hand, the molecular mobility decreases with decreasing $T_{ag}$. Recently, it has been proposed that the shape of the enthalpy of recovery dependence on the aging temperature could be an indication that different regimes are responsible for the structural relaxation.[97] At temperatures close to the glass transition, the relaxation dynamics in PLLA is mostly cooperative, whereas small-scale local motions become predominant with decreasing temperature.[97] A decrease of the activation energy, when going farther in the glassy state, has been reported in polylactide from thermally stimulated depolarization currents.[98] For aging temperatures ranging from −3 up to 50 °C, the curves appear approximately overlapping; so there is no clear effect of the microstructure on the structural relaxation kinetics of the MAF (Fig. 5). These results are consistent with the assumption that this temperature range corresponds to the local motion regime. Indeed, local motions are expected to be less influenced by the presence of crystalline domains than by cooperative motions.[99–102] On the other hand, above 50 °C, *i.e.*, in the segmental motion domain, the curves obtained for amorphous and semi-crystalline PLLAs do not superimpose. This should be related to the differently hindered cooperative motions in the MAF. As an example, above 50 °C, the RAF disturbs the molecular dynamics in the MAF. It contributes to decreasing the scale of cooperative motions, and shifting the glass transition to higher temperatures.[90]

Androsch *et al.*[92] recently investigated the impact of the crystalline morphology on the structural relaxation in polyamide 11. They found that the crystalline morphology strongly impacts the enthalpy of recovery for annealing temperatures slightly below the glass transition, whereas it has a minor impact when physical aging is performed far below the glass transition. They suggested the possible existence of different mechanisms involved in the structural relaxation, in consistence with our results.[92]

To investigate how the structural relaxation kinetics of the MAF is influenced by the microstructure in the segmental motion regime, physical aging experiments have been performed for various times at 63 and 50 °C, *i.e.*, very close to the glass transition, and at the maximum of the $\Delta H$ ($T_{ag}$, $t_{ag}$ = 10 min), respectively. The FSC curves of amorphous and semi-crystalline PLLAs after aging times ranging from 0.001 up to 1000 minutes are presented in Fig. 6. Classically, the peak of enthalpy of recovery shifts to higher temperatures, and it increases in intensity, with the aging time. One can observe that the equilibrium seems to be quickly reached for all samples when performing aging at 63 °C. On the other hand, by aging at 50 °C, the enthalpy loss continues to increase progressively.

In Fig. 7, the enthalpy of recovery values are reported as a function of aging time. For an aging temperature equal to 63 °C, one can observe that amorphous PLLA reaches equilibrium in the shortest time, after 0.01 min of aging, while 10 min of aging is needed to reach equilibrium in semi-crystalline PLLA. Two hypotheses could be considered. This might be the signature of a slower structural relaxation rate in semi-crystalline PLLA, or it might only be caused by a higher distance to equilibrium, *i.e.*, higher total enthalpy loss. Aging at 50 °C helps to reveal that amorphous and semi-crystalline PLLAs follow the same line, from 0.001 up to 10 minutes aging. This evidences that the initial structural relaxation rate is the same in the MAF of amorphous and semi-crystalline PLLAs at 50 °C, in consistence with the results obtained at $T_{ag}$ = 63 °C.

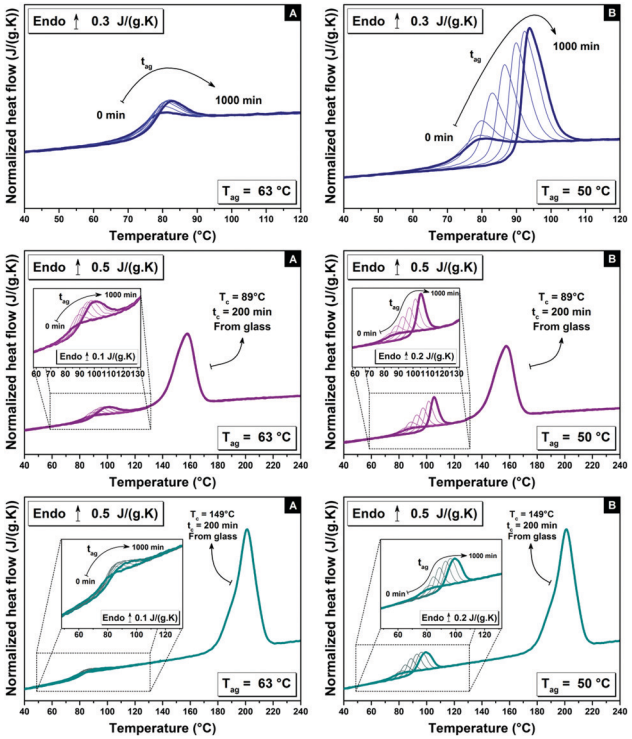


Fig. 6 Heat flow curves normalized to both sample mass and heating rate of initially amorphous PLLA (top) and PLLA crystallized from glass for 200 minutes at $T_c$ = 89 °C (middle) and $T_c$ = 149 °C (bottom) recorded after aging for $t_{ag}$ = [0.001, 0.01, 0.1, 1, 10, 100, and 1000] minutes at $T_{ag}$ = 63 °C (A) and $T_{ag}$ = 50 °C (B). A focus on the glass transition for semi-crystalline PLLA is given in the insets. The curves for non-aged samples are also presented.

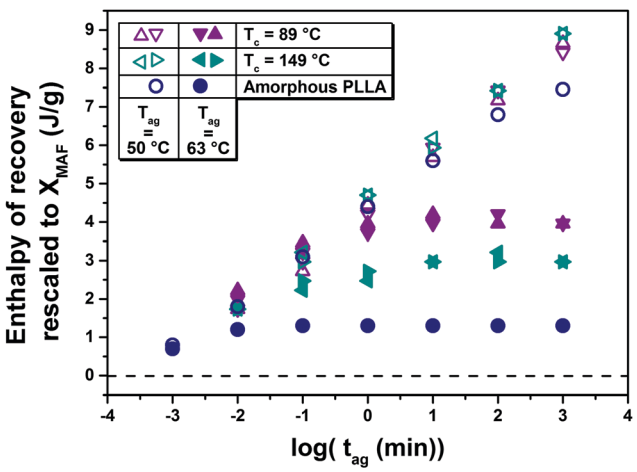


Fig. 7 Enthalpy of recovery rescaled to the content of mobile amorphous fraction as a function of aging time for amorphous and semi-crystalline PLLAs.

It is only after 100 minutes aging that the behaviour of amorphous PLLA starts deviating from the general trend, likely because it approaches equilibrium. These results are consistent with previous investigations from standard DSC measurements, showing that the complex interconnection existing between

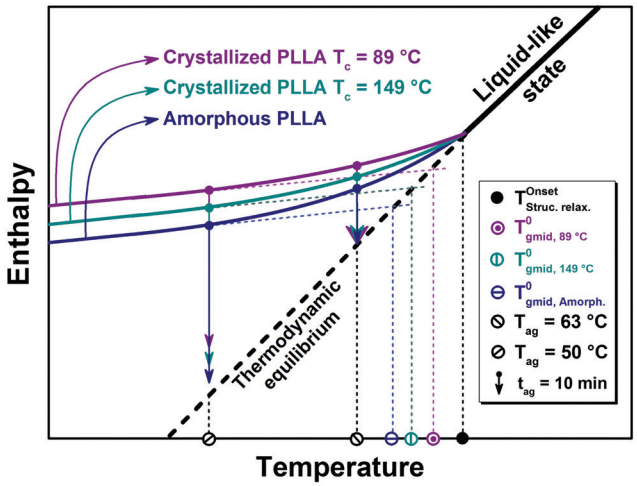


Fig. 8 Schematic representation of the microstructure influence on the structural relaxation process of PLLA from FSC investigations.

amorphous and crystalline phases in spherulites weakly influences the dynamics of structural relaxation processes.[91]

The way by which the structural relaxation in the MAF is influenced by the crystallization conditions in the segmental motion regime is summarized in Fig. 8. While independent of the microstructure, all PLLAs leave the liquid-like state at the same temperature, which corresponds to the onset of structural relaxation; the glass transition midpoint is a function of the coupling between amorphous and crystal. As a consequence, for a given aging temperature, the total enthalpy loss is the lowest for amorphous PLLA and the highest for PLLA crystallized at 89 °C. Since the structural relaxation rate is the same at 63 and 50 °C, and also between samples, the observation that PLLA crystallized at 89 °C needs more time to reach equilibrium may be fully attributed to its higher distance to equilibrium.

### 3.3 The contribution of the rigid amorphous fraction (RAF) to the structural relaxation

Rescaling the values of enthalpy of recovery to the MAF content is a procedure that does not take into account the possibility that the RAF also contributes to the structural relaxation. Despite its lower mobility, RAF should also minimize its excess of enthalpy. Moreover, at temperatures far below the glass transition, RAF and MAF are hardly discriminated, since the whole amorphous phase could be depicted as a solid. Therefore, one could consider that the amorphous phase participates in totality in the structural relaxation.[68] In a recent study,[97] it has been suggested that at high undercooling, structural relaxation occurs only through short-range motions both in the MAF and RAF regions. In Fig. 9, this hypothesis is tested: the values of enthalpy of recovery are presented after rescaling to the whole content of amorphous phase.

For aging temperatures below 55 °C, the enthalpy lost by semi-crystalline samples is significantly lower, with this effect being more pronounced for PLLA crystallized at 89 °C. This evidences that the RAF dramatically slows down the relaxation process. Interestingly, $\Delta H$ ($T_{ag}$, $t_{ag}$ = 10 min) tends to converge

 

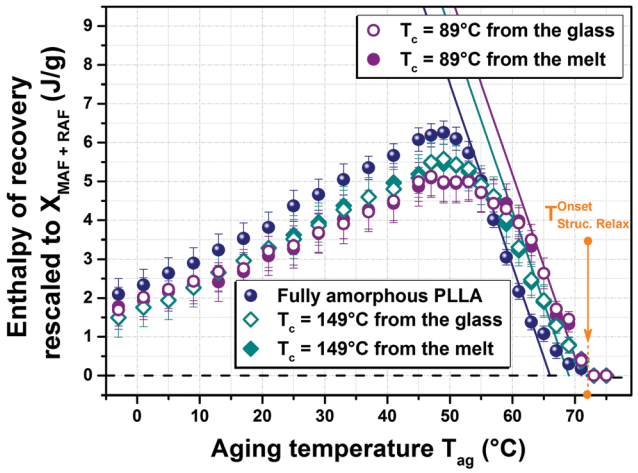


Fig. 9 Enthalpy of recovery rescaled to the sum of mobile and rigid amorphous fractions as a function of aging temperature for amorphous and semi-crystalline PLLAs ($t_c$ = 200 minutes) aged for $t_{ag}$ = 10 minutes. The onset of structural relaxation at 72 °C is indicated by an arrow. The solid lines correspond to the variations of the total enthalpy loss with the aging temperature.

towards the values recorded for amorphous PLLA when decreasing the aging temperature down to −3 °C. This means that far below the glass transition, the structural relaxation kinetics in both MAF and RAF are identical. One can assume that the disappearance of cooperative motions occurs progressively in the MAF from $T_{ag}$ = 50 °C down to $T_{ag}$ = −3 °C. It was identified that when $T_{g\,mid} - T_{ag}$ exceeds 55 °C, exclusively local motions produce structural relaxation in PLLA.[97] Thus, MAF and RAF should relax concomitantly.

For aging temperatures above 55 °C, it is expected that the structural relaxation dynamics strongly differ between RAF and MAF because the latter can participate in cooperative motions, whereas the former cannot. In other terms, the RAF is non-crystalline but it does not participate in the segmental process. As shown in Fig. 10, by including the participation of RAF in the

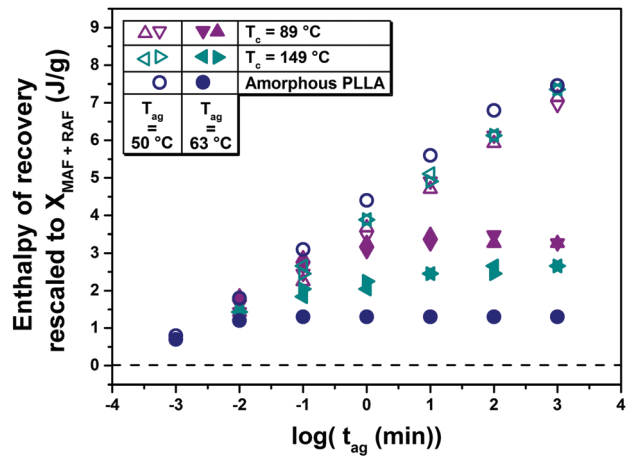


Fig. 10 Enthalpy of recovery rescaled to the whole content of amorphous phase as a function of aging time for amorphous and semi crystalline PLLAs.

physical aging, the kinetics is slower for semi-crystalline samples, in particular for PLLA crystallized at 89 °C. It has been observed above that the structural relaxation rate of the MAF is independent of the microstructure and is the same in the whole segmental motion regime. Consequently, this difference in terms of kinetics could reveal not only that the relaxation occurs at a much slower rate in the RAF, but also that the relaxation of each amorphous fraction is governed by different mechanisms. This is consistent with the assumption that only local motions are allowed in the RAF due to the constraining effect of the neighbouring crystals. This also implies that the MAF relaxation should occur, thanks to local motions, far below the glass transition, when both fractions exhibit the same relaxation kinetics.

## 4. Conclusions

FSC offers a good compromise for physical aging experiments between the time to reach equilibrium that must be sufficiently short to be compatible with a laboratory timescale, and the distance to equilibrium that must be sufficiently high to highlight possible differences in aging rate related to the microstructure. Taking benefit of this, we investigated in this study how quiescent crystallization conditions impact the physical aging of semi-crystalline PLLA. It is proposed that a fair rescaling of the enthalpy of recovery in semi-crystalline PLLA would consider the participation of the RAF. By comparing the structural relaxation rate between MAF and RAF, we deduced that several dynamics are involved in the structural relaxation of the MAF.

In the temperature domain situated slightly below the glass transition, for which segmental motions are allowed, the process is driven by the distance to equilibrium. This one is farther in semi-crystalline PLLA for which the induced microstructure hinders the molecular dynamics strongly enough to shift the glass transition midpoint to higher temperature. The relaxation rate of the MAF is the same between samples. Moreover, it does not depend on the temperature, meaning that the time to reach equilibrium is directly correlated to the total enthalpy loss.

In contrast, the RAF, which is farther from its devitrification temperature, is not involved in the cooperative relaxation and contributes to the physical aging to a lesser extent. The relaxation dynamics are so distinct in this domain between RAF and MAF that they are easily separated. However, these observations are not valid anymore when physical aging is performed at temperatures low enough. Structural relaxation proceeding thanks to local motions arises identically in both RAF and MAF, indistinguishable in terms of mobility, behaving as a solid amorphous phase. Therefore, the quiescent crystallizations performed in this study confirm that the structural relaxation motions in the MAF evolve from segmental to local when decreasing the temperature of aging. This could contribute to the discussion regarding the nature of equilibration mechanisms associated with the physical aging.

## Conflicts of interest

There are no conflicts to declare.

## Acknowledgements

The authors would like to thank Dr Daniele Cangialosi for allowing Dr Xavier Monnier to perform the experiment shown in ESI† concerning the determination of the glass transition temperature upon cooling, thanks to the Flash DSC 1 from the Polymer and Soft Matter Group in the Material Physics Center (MPC). The authors gratefully thank Dr Maria Cristina Righetti from CNR-IPCF as a contributor to the early development of this work, and for her comments, both critical and fruitful, regarding the interpretation of the results.

## References

1 F. Paolucci, D. Baeten, P. C. Roozemond, B. Goderis and G. W. M. Peters, *Polymer*, 2018, **155**, 187–198.
2 J. E. K. Schawe, *Thermochim. Acta*, 2015, **603**, 85–93.
3 K. Jariyavidyanont, R. Androsch and C. Schick, *Polymer*, 2017, **124**, 274–283.
4 R. Androsch, C. Schick and J. W. P. Schmelzer, *Eur. Polym. J.*, 2014, **53**, 100–108.
5 J. E. K. Schawe, P. Pötschke and I. Alig, *Polymer*, 2017, **116**, 160–172.
6 N. G. Perez-de-Eulate, V. Di Lisio and D. Cangialosi, *ACS Macro Lett.*, 2017, **6**, 859–863.
7 S. Gao and S. L. Simon, *Thermochim. Acta*, 2015, **603**, 123–127.
8 E. Lopez and S. L. Simon, *Macromolecules*, 2016, **49**, 2365–2374.
9 Y. P. Koh, S. Gao and S. L. Simon, *Polymer*, 2016, **96**, 182–187.
10 Y. P. Koh, L. Grassia and S. L. Simon, *Thermochim. Acta*, 2015, **603**, 135–141.
11 X. Monnier, A. Saiter and E. Dargent, *Thermochim. Acta*, 2017, **648**, 13–22.
12 S. L. Simon and Y. P. Koh, The glass transition and structural recovery using flash DSC, in *Fast Scanning Calorimetry*, ed. C. Schick and V. Mathot, Springer International Publishing, Switzerland, 2016, pp. 433–459.
13 Y. P. Koh and S. L. Simon, *Polymer*, 2018, **143**, 40–45.
14 Y. P. Koh and S. L. Simon, *J. Chem. Phys.*, 2017, **146**, 203329.
15 S. Gao, Y. P. Koh and S. L. Simon, *Macromolecules*, 2013, **46**, 562–570.
16 X. Monnier, A. Saiter and E. Dargent, *Thermochim. Acta*, 2017, **658**, 47–54.
17 X. Monnier, S. Fernandes Nassar, S. Domenek, A. Guinault, C. Sollogoub, E. Dargent and N. Delpouve, *Polymer*, 2018, **150**, 1–9.
18 H. Yoon, Y. P. Koh, S. L. Simon and G. B. McKenna, *Macromolecules*, 2017, **50**, 4562–4574.
19 H. Yoon and G. B. McKenna, *Sci. Adv.*, 2018, **4**, eaau5423.
20 Q. Zheng, Y. Zhang, M. Montazerian, O. Gulbiten, J. C. Mauro, E. D. Zanotto and Y. Yue, *Chem. Rev.*, 2019, **119**, 7848–7939.
21 M. Rosa, L. Grassia, A. d'Amore and G. d'Escamard, *Procedia Eng.*, 2016, **167**, 265–269.
22 J. Arranz-Andrés, M. L. Cerrada and E. Perez, *Thermochim. Acta*, 2015, **603**, 116–122.
23 J. Martin, N. Stingelin and D. Cangialosi, *J. Phys. Chem. Lett.*, 2018, **9**, 990–995.
24 L. Grassia, Y. P. Koh, M. Rosa and S. L. Simon, *Macromolecules*, 2018, **51**, 1549–1558.
25 G. B. McKenna and S. L. Simon, *Macromolecules*, 2017, **50**, 6333–6361.
26 L. C. E. Struik, *Polym. Eng. Sci.*, 1977, **17**, 165–173.
27 G. B. McKenna, Glass formation and glassy behaviour, in *Comprehensive polymer science*, ed. C. Booth and C. Price, Pergamon Press, Oxford, 1989, vol. 2, Polymer properties, pp. 311–362.
28 I. M. Hodge, *J. Non-Cryst. Solids*, 1994, **169**, 211–266.
29 J. M. Hutchinson, *Prog. Polym. Sci.*, 1995, **20**, 703–760.
30 A. Q. Tool and C. G. Eicitlin, *J. Am. Ceram. Soc.*, 1931, **14**, 276–308.
31 A. J. Kovacs, Transition vitreuse dans les polymères amorphes. Etude phénoménologique, *Fortschritte Der Hochpolymeren–Forschung. Advances in Polymer Science*, Springer, Berlin, Heidelberg, 1963, vol. 3, pp. 394–507.
32 A. Tool, *J. Am. Ceram. Soc.*, 1946, **29**, 240–253.
33 O. S. Narayanaswamy, *J. Am. Ceram. Soc.*, 1971, **54**, 491–498.
34 C. T. Moynihan, P. B. Macedo, C. J. Montrose, P. K. Gupta, M. A. de Bolt, J. F. Dill, B. E. Dom, P. W. Drake, A. J. Easteal, P. B. Elterman, R. P. Moeller, H. Sasabe and J. A. Wilder, *Ann. NY Acad. Sci.*, 1976, **279**, 15–35.
35 M. D. Ediger, *J. Chem. Phys.*, 2017, **147**, 210901.
36 M. S. Beasley, M. Tylinski, Y. Z. Chua, C. Schick and M. D. Ediger, *J. Chem. Phys.*, 2018, **148**, 174503.
37 J. Zhao, S. L. Simon and G. B. McKenna, *Nat. Commun.*, 2013, **4**, 1783.
38 X. Monnier and D. Cangialosi, *Phys. Rev. Lett.*, 2018, **121**, 137801.
39 D. Cangialosi, A. Alegría and J. Colmenero, *Prog. Polym. Sci.*, 2016, **54–55**, 128–147.
40 S. Napolitano, E. Glynos and N. B. Tito, *Rep. Prog. Phys.*, 2017, **80**, 036602.
41 V. M. Boucher, D. Cangialosi, A. Alegría and J. Colmenero, *Phys. Chem. Chem. Phys.*, 2017, **19**, 961–965.
42 A. Brunacci, J. M. G. Cowie, R. Ferguson, J. L. Gomez Ribelles and A. Vidaurre Garayo, *Macromolecules*, 1996, **29**, 7976–7988.
43 N. R. Cameron, J. M. G. Cowie, R. Ferguson and I. J. McEwen, *Polymer*, 2000, **41**, 7255–7262.
44 L. Andreozzi, M. Faetti, M. Giordano, D. Palazzuoli and F. Zulli, *Macromolecules*, 2003, **36**, 7379–7387.
45 A. Saiter, M. Hess, N. A. D'Souza and J.-M. Saiter, *Polymer*, 2002, **43**, 7497–7504.
46 L. Andreozzi, M. Faetti, M. Giordano and F. Zulli, *Macromolecules*, 2005, **38**, 6056–6067.
47 Y. P. Koh and S. L. Simon, *Macromolecules*, 2013, **46**, 5815–5821.
48 V. M. Boucher, D. Cangialosi, A. Alegría and J. Colmenero, *Macromolecules*, 2011, **44**, 8333–8342.
49 N. G. Perez-De Eulate and D. Cangialosi, *Phys. Chem. Chem. Phys.*, 2018, **20**, 12356–12361.

 

50 D. Cangialosi, V. M. Boucher, A. Alegría and J. Colmenero, *Phys. Rev. Lett.*, 2013, **111**, 095701.
51 N. G. Perez-De Eulate and D. Cangialosi, *Macromolecules*, 2018, **51**, 3299–3307.
52 L. Pradipkanti, M. Chowdhury and D. K. Satapathy, *Phys. Chem. Chem. Phys.*, 2017, **19**, 29263–29270.
53 J. Grenet, E. Bouthegourd, A. Esposito, A. Saiter and J.-M. Saiter, *Philos. Mag.*, 2013, **93**, 2932–2946.
54 B. Atawa, N. Couvrat, G. Coquerel, E. Dargent and A. Saiter, *Mater. Lett.*, 2018, **228**, 141–144.
55 S. Domenek, C. Courgneau and V. Ducruet, Characteristics and applications of PLA, in *Biopolymers: Biomedical and Environmental Applications*, ed. S. Kalia and L. Averous, Wiley, Hoboken, NJ, 2011, pp. 183–223.
56 M. Murariu, A.-L. Dechief, R. Ramy-Ratiarison, Y. Paint, J.-M. Raquez and P. Dubois, *Nanocomposites*, 2015, **1**, 71–82.
57 *Poly(lactic acid): Synthesis, Structures, Properties, Processing, and Applications*, ed. R. A. Auras, L.-T. Lim, S. E. M. Selke and H. Tsuji, John Wiley & Sons, 2011, ch. 27–30, pp. 443–486.
58 R. Androsch and M. L. Di Lorenzo, *Macromolecules*, 2013, **46**, 6048–6056.
59 V. Di Lisio, E. Sturabotti, I. Francolini, A. Piozzi and A. Martinelli, *J. Polym. Sci., Part B: Polym. Phys.*, 2019, **57**, 174–181.
60 L. Cui, B. Imre, D. Tatraaljai and B. Pukanszky, *Polymer*, 2020, **186**, 122014.
61 X. Monnier, L. Chevalier, A. Esposito, L. Fernandez-Ballester, A. Saiter and E. Dargent, *Polymer*, 2017, **126**, 141–151.
62 B. Wunderlich, *Prog. Polym. Sci.*, 2003, **28**, 383–450.
63 S. X. Lu, P. Cebe and M. Capel, *Macromolecules*, 1997, **30**, 6243–6250.
64 C. Schick, A. Wurm and A. Mohammed, *Thermochim. Acta*, 2003, **396**, 119–132.
65 J. Menczel and B. Wunderlich, *J. Polym. Sci., Polym. Lett. Ed.*, 1981, **19**, 261–264.
66 M. Pyda, R. C. Bopp and B. Wunderlich, *J. Chem. Thermodyn.*, 2004, **36**, 731–742.
67 M. C. Righetti and E. Tombari, *Thermochim. Acta*, 2011, **522**, 118–127.
68 M. C. Righetti, M. Gazzano, N. Delpouve and A. Saiter, *Polymer*, 2017, **125**, 241–253.
69 J. Zhang, K. Tashiro, H. Tsuji and A. J. Domb, *Macromolecules*, 2008, **41**, 1352–1357.
70 T. Kawai, N. Rahman, G. Matsuba, K. Nishida, T. Kanaya, M. Nakano, H. Okamoto, J. Kawada, A. Usuki, N. Honma, K. Nakajima and M. Matsuda, *Macromolecules*, 2007, **40**, 9463–9469.
71 J. Zhang, K. Tashiro, A. J. Domb and H. Tsuji, *Macromol. Symp.*, 2006, **242**, 274–278.
72 M. C. Righetti, D. Prevosto and E. Tombari, *Macromol. Chem. Phys.*, 2016, **217**, 2013–2026.
73 S. Fernandes Nassar, A. Guinault, N. Delpouve, V. Divry, V. Ducruet, C. Sollogoub and S. Domenek, *Polymer*, 2017, **108**, 163–172.
74 Y. Yuryev, P. Wood–Adams, M. C. Heuzey, C. Dubois and J. Brisson, *Polymer*, 2008, **49**, 2306–2320.
75 A. Toda and M. Konishi, *Thermochim. Acta*, 2014, **589**, 262–269.
76 K. Jariyavidyanont, A. Abdelaziz, R. Androsch and C. Schick, *Thermochim. Acta*, 2019, **674**, 95–99.
77 J. E. K. Schawe, *Thermochim. Acta*, 2015, **603**, 128–134.
78 M. C. Righetti, M. Gazzano, M. L. Di Lorenzo and R. Androsch, *Eur. Polym. J.*, 2015, **70**, 215–220.
79 J. L. Gomez Ribelles, A. Ribes Greus and R. Diaz Calleja, *Polymer*, 1990, **31**, 223–230.
80 M. Cocca, M. L. Di Lorenzo, M. Malinconico and V. Frezza, *Eur. Polym. J.*, 2011, **47**, 1073–1080.
81 M. Pluta and A. Galeski, *J. Appl. Polym. Sci.*, 2002, **86**, 1386–1395.
82 P. Pan, B. Zhu, W. Kai, T. Dong and Y. Inoue, *J. Appl. Polym. Sci.*, 2008, **107**, 54–62.
83 M. Yasuniwa, S. Tsubakihara, K. Iura, Y. Ono, Y. Dan and K. Takahashi, *Polymer*, 2006, **47**, 7554–7563.
84 Y. Furushima, C. Schick and A. Toda, *Polym. Cryst.*, 2018, **1**, e10005.
85 M. L. Di Lorenzo and R. Androsch, *AIP Conf. Proc.*, 2016, **1736**, 020009.
86 R. Androsch, C. Schick and M. L. Di Lorenzo, *Macromol. Chem. Phys.*, 2014, **215**, 1134–1139.
87 R. Androsch, M. L. Di Lorenzo and C. Schick, *Eur. Polym. J.*, 2016, **75**, 474–485.
88 J. Lin, S. Shenogin and S. Nazarenko, *Polymer*, 2002, **43**, 4733–4743.
89 S. Fernandes Nassar, S. Domenek, A. Guinault, G. Stoclet, N. Delpouve and C. Sollogoub, *Macromolecules*, 2018, **51**, 128–136.
90 A. Saiter, N. Delpouve, E. Dargent, W. Oberhauser, L. Conzatti, F. Cicogna and E. Passaglia, *Eur. Polym. J.*, 2016, **78**, 274–289.
91 N. Delpouve, M. Arnoult, A. Saiter, E. Dargent and J.-M. Saiter, *Polym. Eng. Sci.*, 2014, **54**, 1144–1150.
92 R. Androsch, K. Jariyavidyanont and C. Schick, *Entropy*, 2019, **21**, 984.
93 J. E. K. Schawe, *Thermochim. Acta*, 2015, **603**, 85–93.
94 J. E. K. Schawe, *J. Therm. Anal. Calorim.*, 2017, **127**, 931–937.
95 A. Esposito, N. Delpouve, V. Causin, A. Dhotel, L. Delbreilh and E. Dargent, *Macromolecules*, 2016, **49**, 4850–4861.
96 V. M. Boucher, D. Cangialosi, A. Alegría and J. Colmenero, *Macromolecules*, 2012, **45**, 5296–5306.
97 M. C. Righetti and E. Mele, *Thermochim. Acta*, 2019, **672**, 157–161.
98 S. Araujo, N. Delpouve, A. Dhotel, S. Domenek, A. Guinault, L. Delbreilh and E. Dargent, *ACS Omega*, 2018, **3**, 17092–17099.
99 J. Dobbertin, A. Hensel and C. Schick, *J. Therm. Anal.*, 1996, **47**, 1027–1040.
100 C. Schick, J. Dobbertin, M. Potter, H. Dehne, A. Hensel, A. Wurm, A. M. Ghoneimm and S. Weyer, *J. Therm. Anal.*, 1997, **49**, 499–511.
101 J. Ren and K. Adachi, *Macromolecules*, 2003, **36**, 5180–5186.
102 A. Schönhals, Molecular Dynamics in Polymer Model Systems, in *Broadband Dielectric Spectroscopy*, ed. F. Kremer and A. Schönhals, Springer-Verlag, Berlin, Germany, 2003, pp. 225–293.